

ELECTRONIC SUPPLEMENTARY MATERIAL

***In situ* Synthesis of Nitrogen-doped Carbon Dots in Interlayer Region
of Layered Double Hydroxide with Tunable Quantum Yield**

Wendi Liu, Simin Xu, Ruizheng Liang*, Min Wei*, David G. Evans, and Xue Duan

*State Key Laboratory of Chemical Resource Engineering, Beijing Advanced Innovation
Center for Soft Matter Science and Engineering, Beijing University of Chemical Technology,
Beijing 100029, P. R. China*

* Corresponding authors. Tel: +86-10-64412131; Fax: +86-10-64425385.

E-mail addresses: liangruizheng2000@163.com (R. Liang); weimin@mail.buct.edu.cn (M.
Wei).

Experimental Section

Materials:

Analytical pure $\text{Mg}(\text{NO}_3)_2 \cdot 6\text{H}_2\text{O}$, $\text{Al}(\text{NO}_3)_3 \cdot 9\text{H}_2\text{O}$, NaOH, citric acid, ethylenediamine and hydrochloric acid were purchased from Beijing Chemical Co. Ltd. and used without further purification. Polyvinyl alcohol (PVA, $M_w=77,000$) was purchased from aladdin Chemical Co. Ltd. N,N'-dimethylacrylamide (DMAA) and Darocur 1173 were purchased from Adams Reagent Co. Ltd. The deionized and decarbonated water were used in all the experimental processes.

Synthesis of CA/LDHs:

The citric acid (CA) intercalated LDHs was prepared by using the separate nucleation and aging steps (SNAS) method reported by our group.¹ Typically, 50 mL of solution A ($\text{Mg}(\text{NO}_3)_2 \cdot 6\text{H}_2\text{O}$: 0.02 mol and $\text{Al}(\text{NO}_3)_3 \cdot 9\text{H}_2\text{O}$: 0.01 mol) and 20 mL of solution B (NaOH: 0.07 mol and CA: 0.01 mol) were simultaneously added to a colloid mill with rotor speed of 3000 rpm and blend for 1 min. CA/LDHs materials with various $\text{Mg}^{2+}/\text{Al}^{3+}$ molar ratios were prepared by adjusting the feed quantity of $\text{Mg}(\text{NO}_3)_2 \cdot 6\text{H}_2\text{O}$ from 0.02 mol to 0.10 mol (with $\text{Mg}^{2+}/\text{Al}^{3+}$ ratio of 2–5), and increasing the feed quantity of NaOH accordingly. Then the colloid suspension was transferred into a teflon-lined stainless steel autoclave and aged at 110 °C for 24 h. The product was centrifuged and washed 3 times with distilled water and ethanol followed by drying in an oven at 60 °C for 12 h.

Synthesis of N-CDs/LDHs:

CA/LDH (0.1000 g) and ethylenediamine (50 μL) were dissolved in deionized water (10 mL). After an ultrasonic dispersion for 60 s, the suspension was transferred into a teflon-lined

autoclave (20 mL) followed by a heat treatment at 150 °C for 6 h. After the reaction, the autoclave was cooled to room temperature. Then the product was purified by centrifugation and dried in an oven at 60 °C for 4 h. To obtain the pure N-CDs generated in the LDH gallery during hydrothermal reaction, the N-CDs/LDHs sample was dissolved in concentrated hydrochloric acid (1 M), followed by a dialysis operation for 24 h.

Preparation of N-CDs/LDH@PVA thin film and N-CDs/LDH@PDMAA bulk material:

PVA (0.4 g) was dispersed in deionized water (9.6 g) under stirring for 4 h, followed by the addition of N-CDs/LDH (0.05 g). After ultrasonic dispersion for 300 s, 5 mL of the mixed suspension was dropped onto the surface of a watch-glass, and then was dried at 40 °C in an oven to obtain the fluorescent film.

For the preparation of N-CDs/LDH@PDMAA bulk material, after fully blending of N-CDs/LDH (0.05 g) in 5 mL of DMAA, Darocur 1173 (50 µl) was added as an initiator. The mixture was then poured in a nummular mould and exposed under a 2 kW of UV radiation for 2 h.

Computational details

Model construction:

Four models, named as CA/2-LDH, CA/3-LDH, CA/4-LDH, and CA/5-LDH, respectively, were constructed according to the chemical compositions of these samples. The chemical formulae of CA/2-LDH, CA/3-LDH, CA/4-LDH and CA/5-LDH are $\text{Mg}_{200}\text{Al}_{124}(\text{OH})_{648}(\text{C}_6\text{H}_6\text{O}_7)_{29}(\text{C}_6\text{H}_5\text{O}_7)_{22}$, $\text{Mg}_{218}\text{Al}_{106}(\text{OH})_{648}(\text{C}_6\text{H}_6\text{O}_7)_{14}(\text{C}_6\text{H}_5\text{O}_7)_{26}$, $\text{Mg}_{236}\text{Al}_{88}(\text{OH})_{648}(\text{C}_6\text{H}_6\text{O}_7)_7(\text{C}_6\text{H}_5\text{O}_7)_{26}$ and $\text{Mg}_{255}\text{Al}_{69}(\text{OH})_{648}(\text{C}_6\text{H}_5\text{O}_7)_{23}$, respectively, which are the same with the experimental observations. The space group for these four models is $\bar{p}3m1$,² which is commonly used for LDHs

materials. The unit cell parameters were set as $\alpha = \beta = 90^\circ$, $\gamma = 120^\circ$. The other three unit cell parameters, a , b , and c were referred to the powder X-ray diffraction observations. The molar ratios of Mg:Al in these four models are 1.613, 2.057, 2.682 and 3.696, respectively.

Computational method:

In this work, the molecular dynamics (MD) simulations were performed employing the force field of LDHFF³ in isothermal-isobaric (NPT) ensemble, with the temperature of 298 K and the pressure of 0.1 MPa. Temperature and pressure control were carried out utilizing the Andersen method⁴ and the Berendsen method,⁵ respectively. The Ewald summation technique⁶ was applied to calculate the long-range Coulombic interactions. The van der Waals interactions were calculated with a “spline-cutoff” method. The time step is 1 fs, which is common for the characterization of thermal motion. These MD simulations were carried out using the Forcite module in the Materials Studio version 5.5 software package (Accelrys Software Inc.: San Diego, CA). For these four models, MD simulations of 10 ns were performed. All models can reach equilibrium within 1 ns according to the temperature and pressure. The dynamic trajectories of the last 4 ns⁷ were recorded every 10 ps for these four models to calculate the diffusion coefficient with the Einstein equation⁸:

$$D = \lim_{t \rightarrow \infty} \frac{1}{2t} \langle (r_0 - r_t)^2 \rangle \quad (1)$$

where t is time; r_t represents the Cartesian position vector of EDA at corresponding time t ; and the term into bracket is the mean squared displacement of EDA.

Sample Characterization

X-ray diffraction patterns (XRD) were recorded by using a Rigaku 2500VB2+PC diffractometer under the conditions: 40 kV, 50 mA, Cu K α radiation ($\lambda=0.154056$ nm) with step-scanned in step of 0.04° (2θ) in the range from 3 to 70° . X-ray photoelectron spectra (XPS)

were performed on a Thermo VG ESCALAB 250 X-ray photoelectron spectrometer using Al K α X-rays as the excitation source. The Fourier transform infrared (FT-IR) spectra were recorded by a Nicolet 605 XB FT-IR spectrometer in the range 4000–400 cm⁻¹ with 2 cm⁻¹ resolution. The morphology was investigated by using a scanning electron microscope (SEM Hitachi S-3500) equipped with an EDX attachment (EDX Oxford Instrument Isis 300), and the applied accelerating voltage was 20 kV. TEM images were recorded on a JEOL JEM-2100 transmission electron microscope with the accelerating voltage of 200 KV. The thickness data were obtained by using the Veeco NanoScope IIIa atomic force microscope (AFM). Raman measurements were carried out with excitation of 633 nm by using a confocal Raman microspectrometer (Renishaw, inVia-Reflex). The fluorescence emission and excitation spectra were performed on a RF-5301PC fluorospectrophotometer. 3D fluorescence data were recorded by HITACHI F-7000 fluorescence spectrophotometer. Photoluminescence quantum yield (PLQY) was measured by using a Nanolog FL3-2iHR infrared fluorescence spectrometer equipped with an integrating sphere. The elemental content of Mg and Al in samples was determined by inductively coupled plasma (ICP) emission spectroscopy on a Shimadzu ICPS-7500 instrument. The organic elemental analysis were carried out by a Perkin Elmer Elementarvario elemental analysis instrument. Temperature-dependent fluorescence spectra of N-CDs/LDH were detected by Craic 20/30 PV microspectrophotometer. Confocal microscopy images were taken using Leica TCS sp8 confocal laser scanning platform. The emission spectra and color coordinates of BLED were determined by Konica Minolta CS-2000 spectroradiometer.

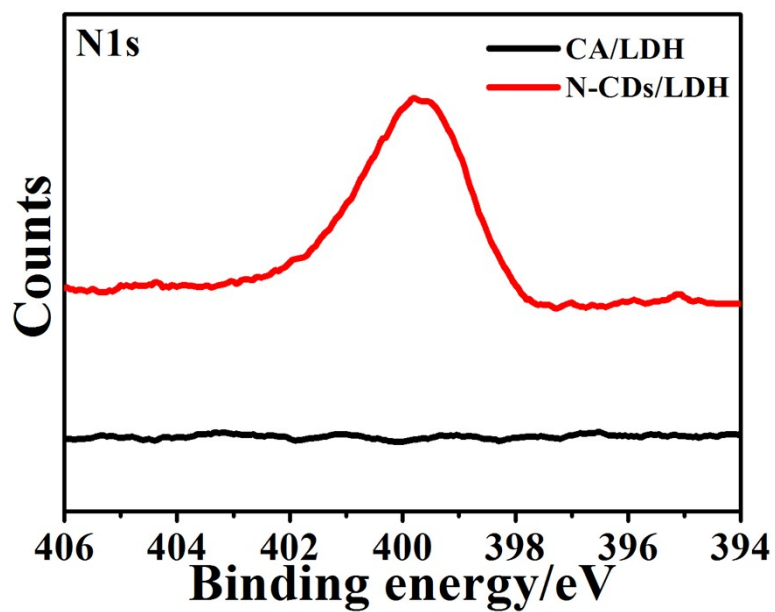


Figure S1. N1s XPS spectra of CA/LDH and N-CDs/LDH, respectively.

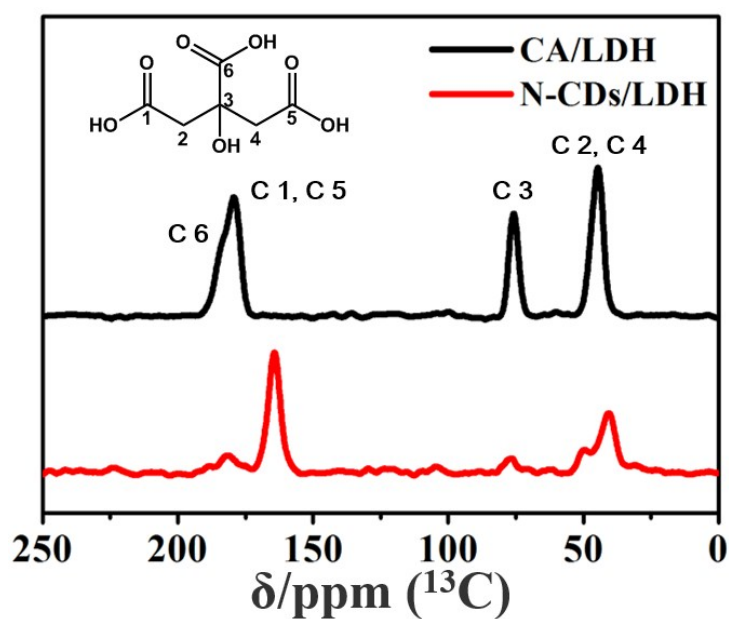


Figure S2. ¹³C MAS NMR spectra of CA/LDH and N-CDs/LDH, respectively.

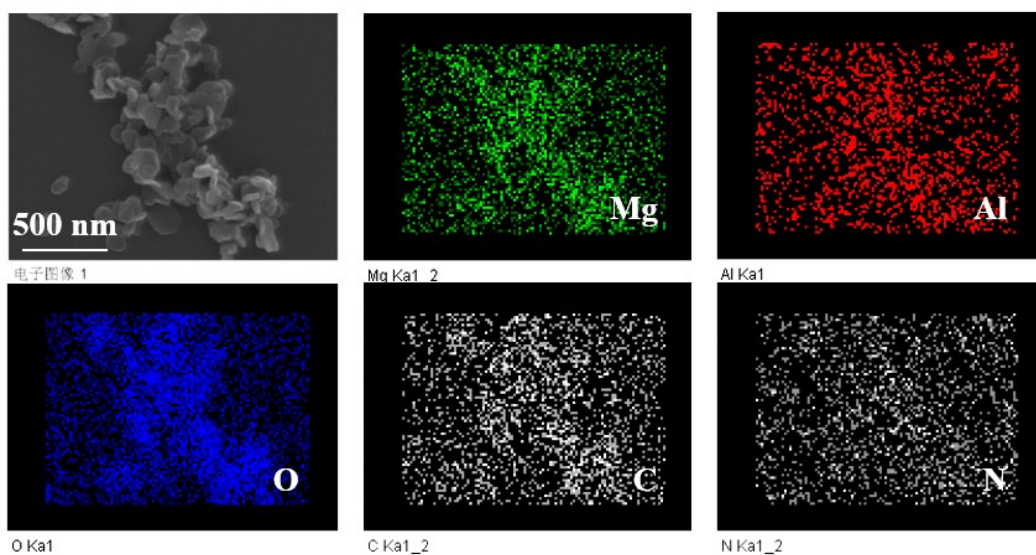


Figure S3. EDS mapping images of N-CDs/LDH composite material.

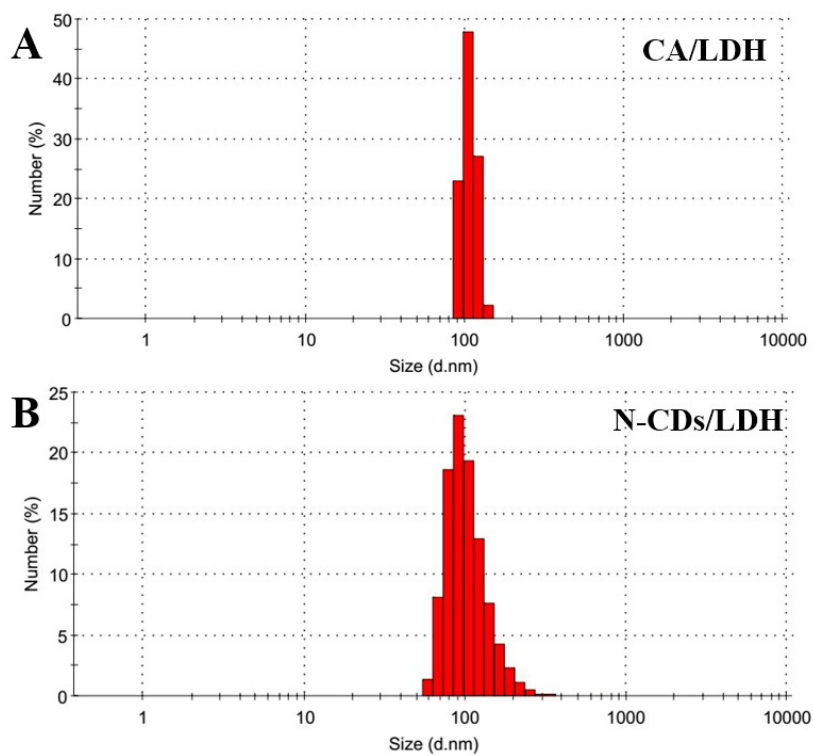


Figure S4. Particle size distribution of (A) CA/LDH and (B) N-CDs/LDH.

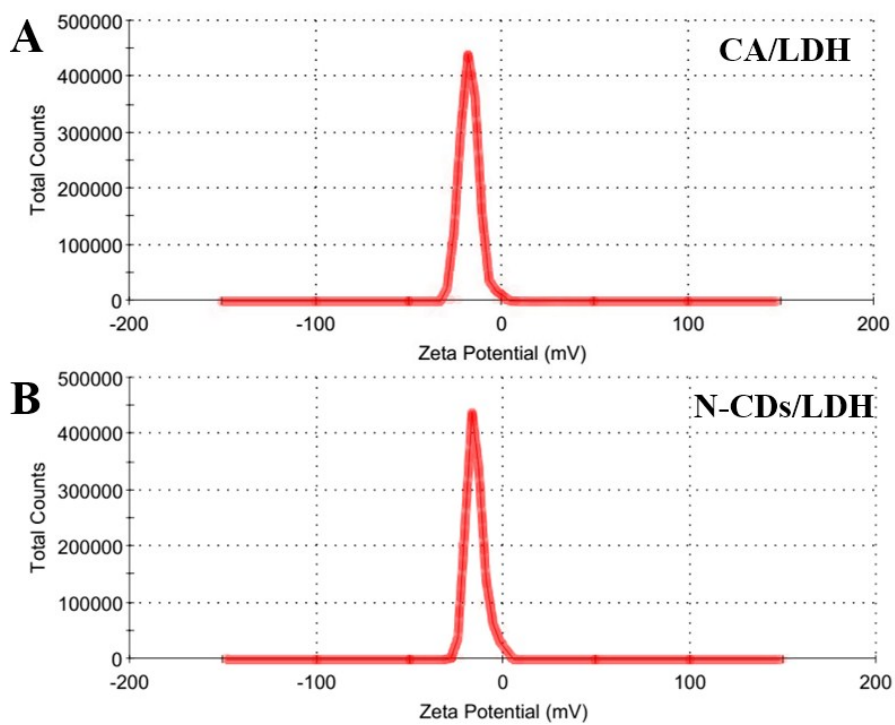


Figure S5. Zeta potential distribution of (A) CA/LDH and (B) N-CDs/LDH.

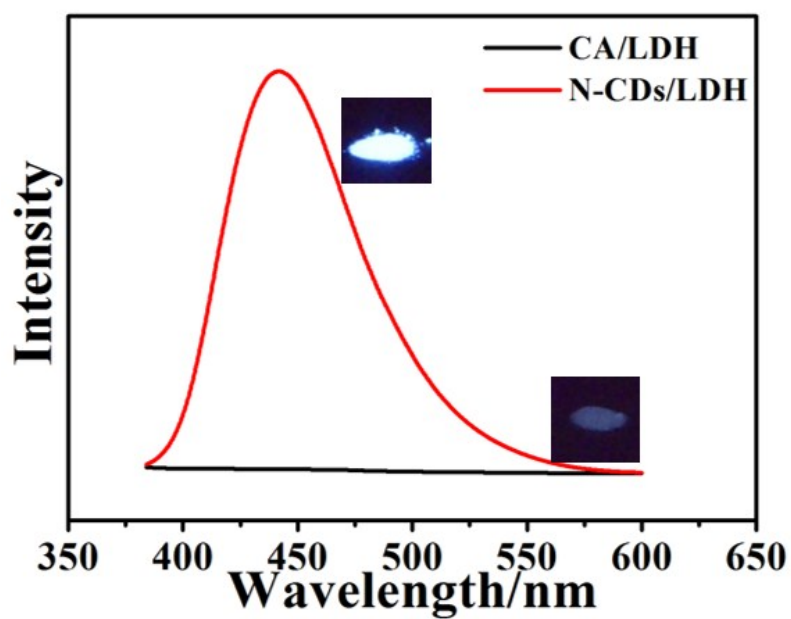


Figure S6. Fluorescence spectra of CA/LDH and N-CDs/LDH; the insets show corresponding photographs under UV light.

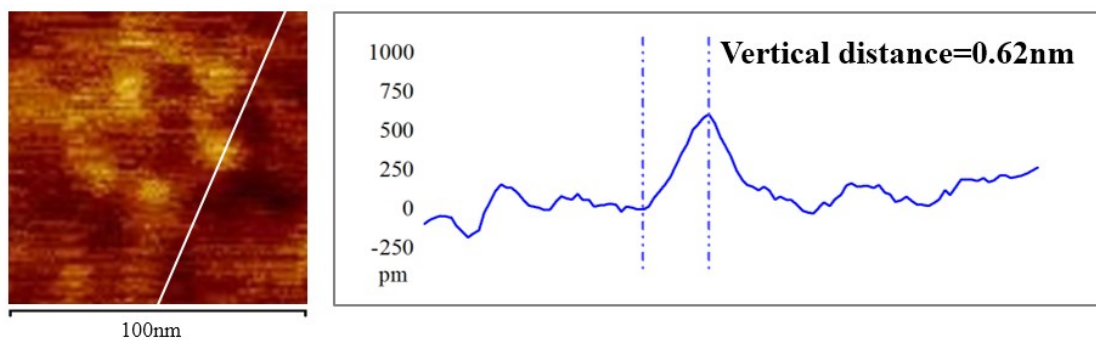


Figure S7. AFM image and corresponding height profile of N-CDs.

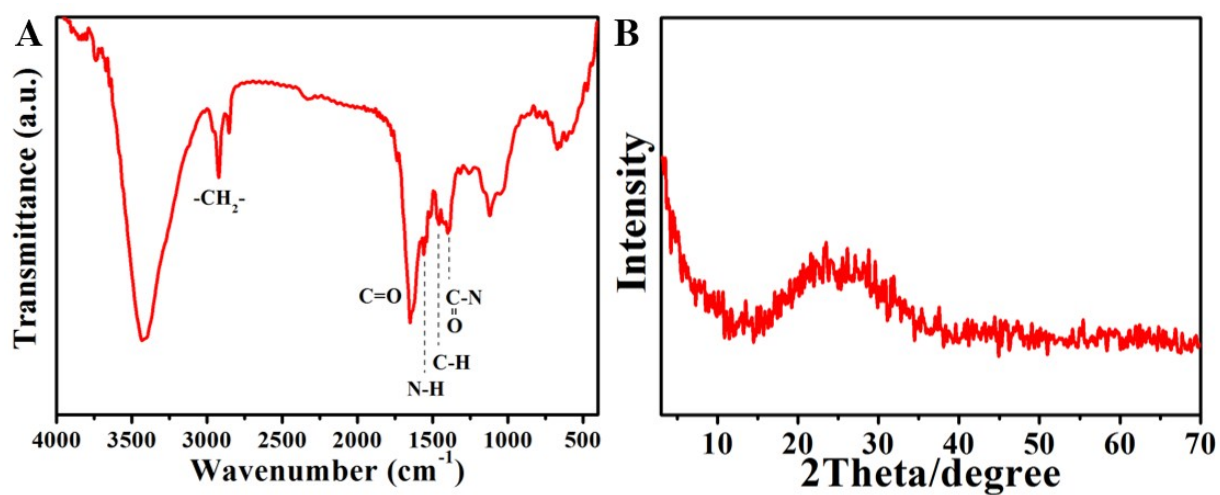


Figure S8. (A) FT-IR spectrum and (B) XRD pattern of N-CDs.

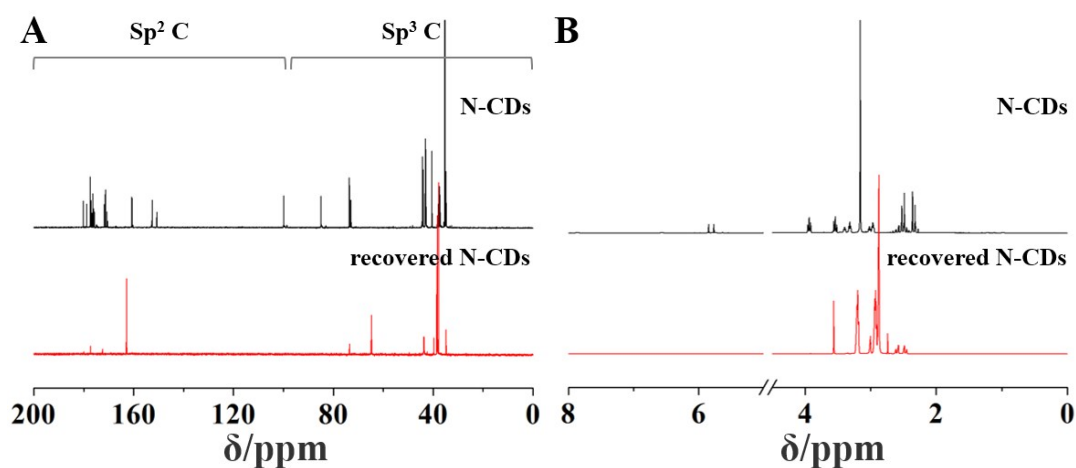


Figure S9. (A) $^1\text{H-NMR}$ and (B) $^{13}\text{C-NMR}$ spectra of N-CDs prepared by conventional hydrothermal method and 2D interlayer reaction.

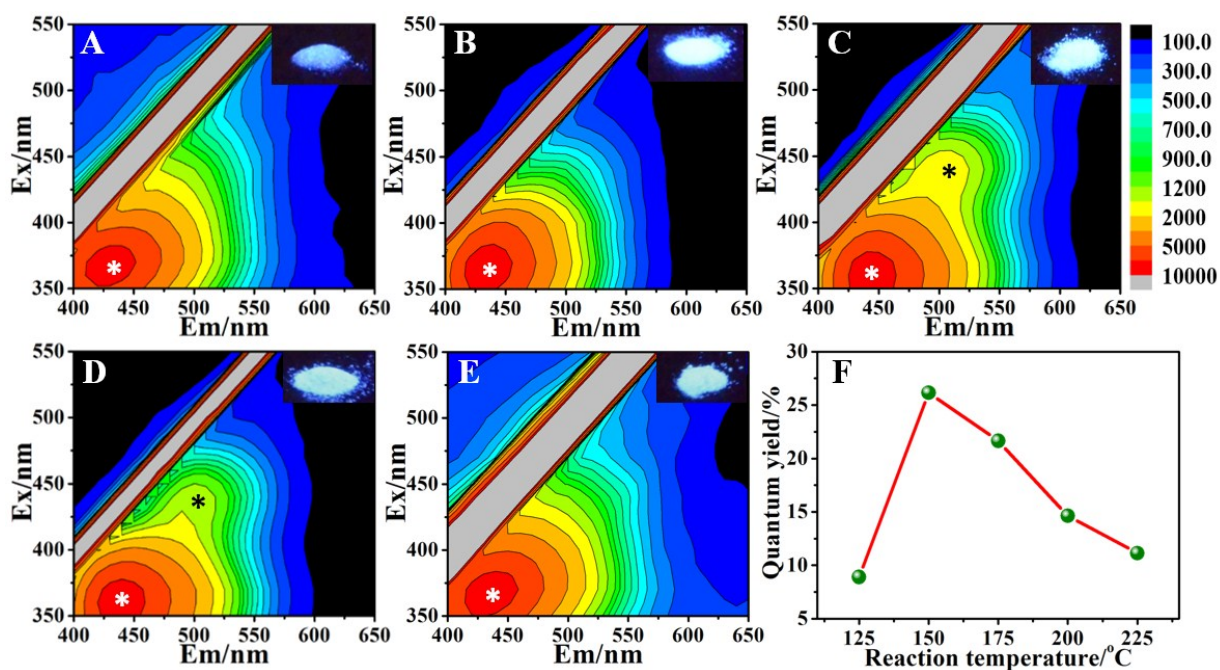


Figure S10. 3D fluorescence spectra of N-CDs/LDH materials obtained at various reaction temperatures: (A) 125 °C, (B) 150 °C, (C) 175 °C, (D) 200 °C and (E) 225 °C; the insets show corresponding photographs under UV light; (F) PLQY of these N-CDs/LDH materials.

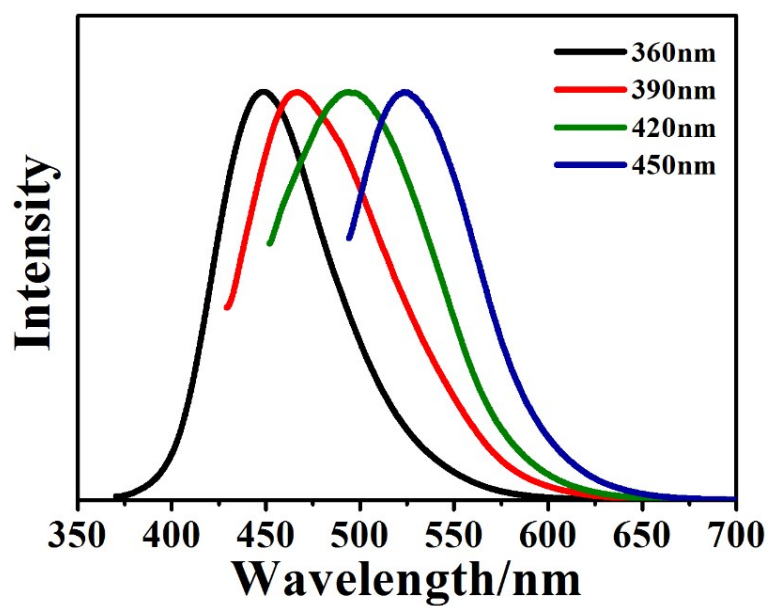


Figure S11. Normalized emission spectra of N-CDs/LDH (reaction temperature: 175 °C) with various excitation wavelength.

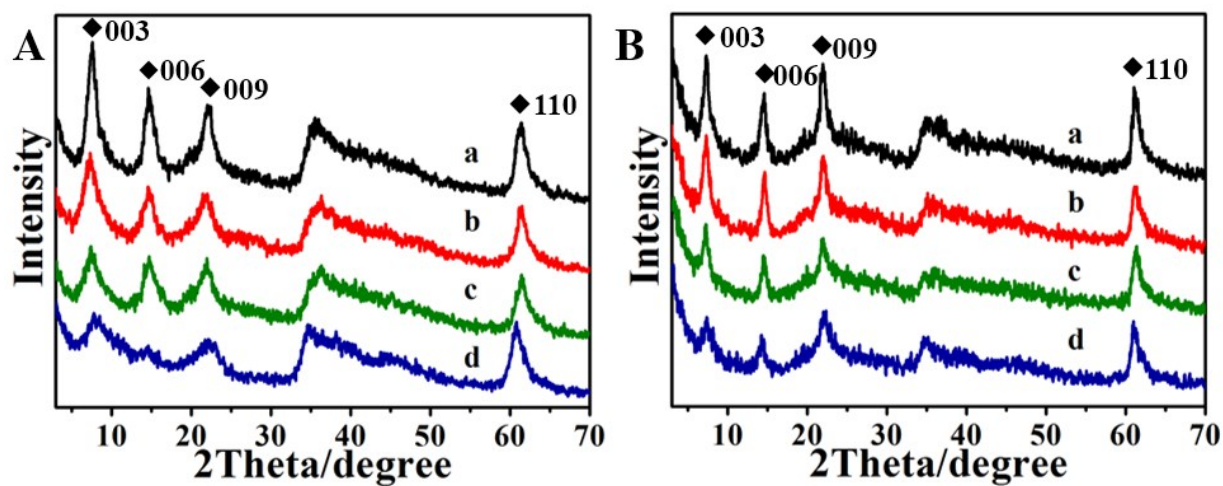


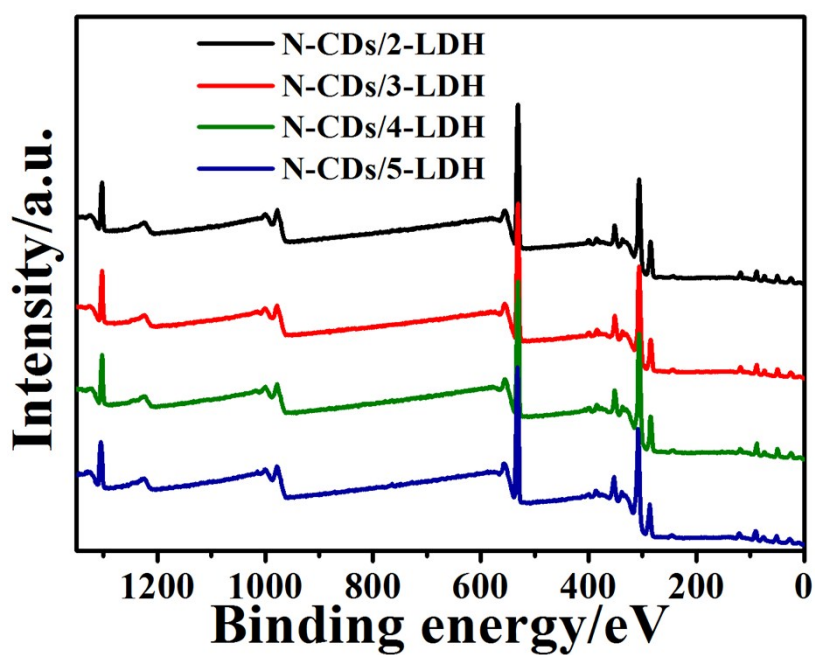
Figure S12. XRD patterns of CA/*X*-LDH (A) and N-CDs/*X*-LDH (B) (a: *X*=2; b: *X*=3; c: *X*=4; d: *X*=5).

Table S1. Quantum yields (QYs) of CDs-based solid-state fluorescent materials

Sample	QY/%	Ref.
CDs/silica	13	9
CDs/DAA	15.7	10
Si-CDs/gel glass	16–88	11
N-doped CDs	10.1	12
CDs/PEG	12.6	13
CDs/starch	50	14
CDs/silica glass	61	15
Si-CDs/SiO ₂	0.1–6.7	16
CDs/polymer	18	17
B-doped CDs	18	18
CDs/silsesquioxane	60	19
N-doped CDs	35	20

Table S2. Elemental analysis results of CA/*X*-LDH and N-CDs/*X*-LDH (*X*=2–5)

Sample	N [wt.%]	C [wt.%]	H [wt.%]	N/C
CA/2-LDH	<0.05	12.6	4.24	-
CA/3-LDH	<0.05	10.7	3.98	-
CA/4-LDH	<0.05	8.89	4.08	-
CA/5-LDH	<0.05	7.13	3.95	-
N-CDs/2-LDH	0.48	11.1	4.34	0.043
N-CDs/3-LDH	0.55	9.70	4.14	0.057
N-CDs/4-LDH	0.67	7.34	4.19	0.091
N-CDs/5-LDH	0.76	6.58	4.19	0.12

**Figure S13.** XPS spectra of N-CDs/*X*-LDH (*X*=2–5) samples.

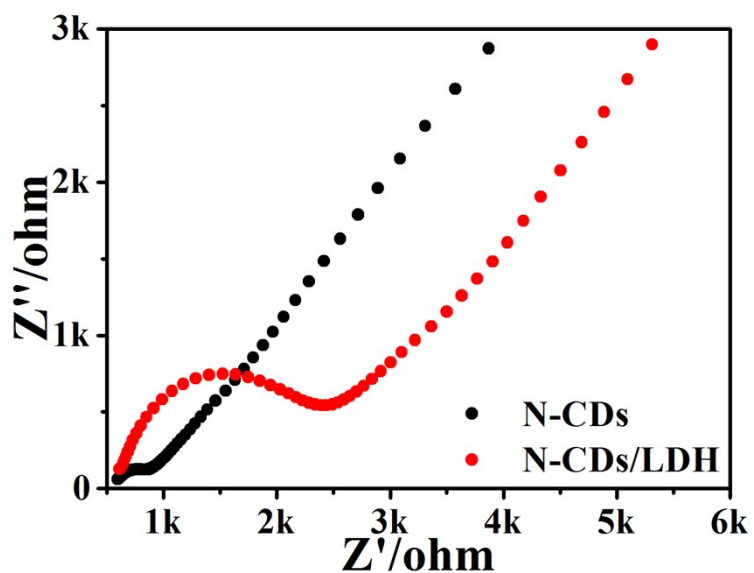


Figure S14. Nyquist plots of electrochemical impedance spectroscopy for the interlayer generated N-CDs and N-CDs/LDH composite, respectively.

Table S3. Mg^{2+}/Al^{3+} ratio of CA/X-LDH ($X=2-5$) samples according to inductively coupled plasma atomic emission spectroscopy (ICP-AES) results

Sample	CA/2-LDH	CA/3-LDH	CA/4LDH	CA/5-LDH
Mg^{2+}/Al^{3+} ratio	1.610	2.064	2.660	3.680

Table S4. Chemical compositions and charge density of CA/*X*-LDH (*X*=2–5) samples

Sample	Chemical composition	Chemical composition (extended)	Charge density ($q_e/\text{\AA}^2$)
CA/2-LDH	$\text{Mg}_{0.617}\text{Al}_{0.383}(\text{OH})_2\text{CA}_{0.156}$	$\text{Mg}_{200}\text{Al}_{124}(\text{OH})_{648}\text{CA}_{51}$	2.98
CA/3-LDH	$\text{Mg}_{0.674}\text{Al}_{0.326}(\text{OH})_2\text{CA}_{0.123}$	$\text{Mg}_{218}\text{Al}_{106}(\text{OH})_{648}\text{CA}_{40}$	2.54
CA/4-LDH	$\text{Mg}_{0.727}\text{Al}_{0.273}(\text{OH})_2\text{CA}_{0.096}$	$\text{Mg}_{236}\text{Al}_{88}(\text{OH})_{648}\text{CA}_{31}$	2.13
CA/5-LDH	$\text{Mg}_{0.786}\text{Al}_{0.214}(\text{OH})_2\text{CA}_{0.072}$	$\text{Mg}_{255}\text{Al}_{69}(\text{OH})_{648}\text{CA}_{23}$	1.67

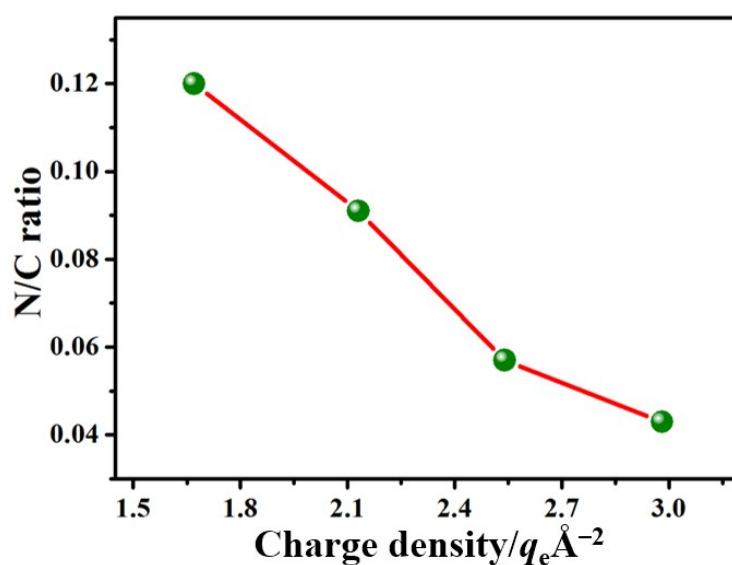


Figure S15. N/C molar ratio of N-CDs/*X*-LDH (*X*=2–5) samples as a function of charge density of LDH host layer.

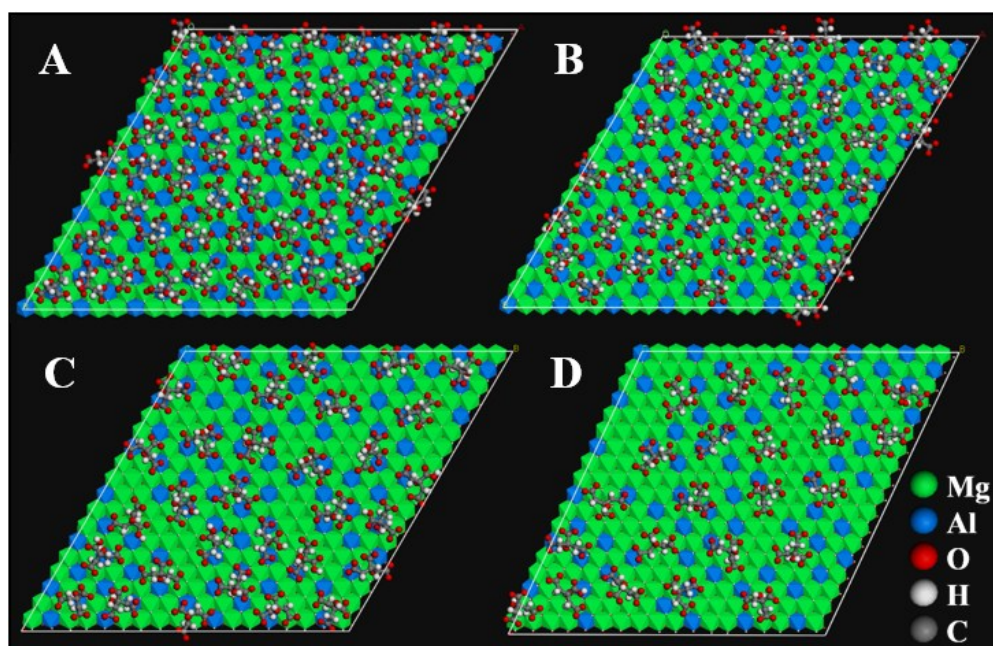


Figure S16. Snapshots of CA/2-LDH (A), CA/3-LDH (B), CA/4-LDH (C) and CA/5-LDH (D) after 5 nanoseconds of molecular dynamics simulation.

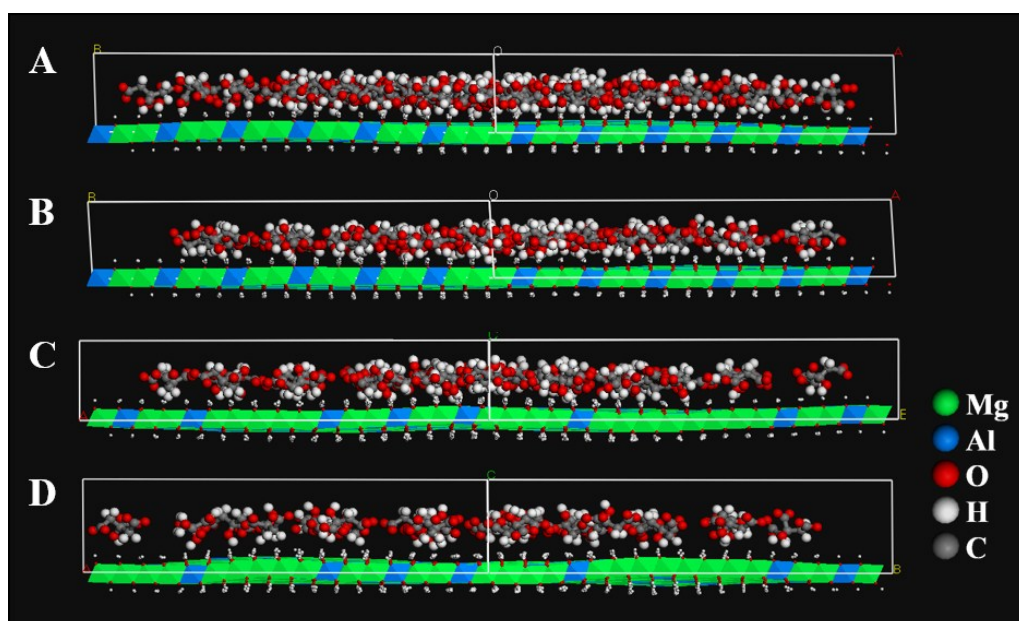


Figure S17. Side-view snapshots of CA/2-LDH (A), CA/3-LDH (B), CA/4-LDH (C) and CA/5-LDH (D) after 5 nanoseconds of molecular dynamics simulation.

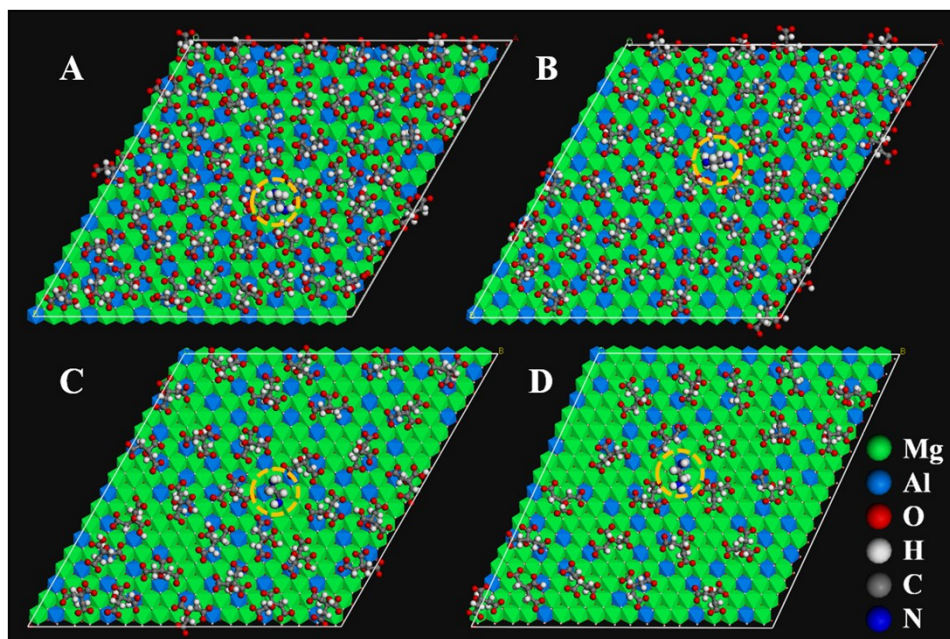


Figure S18. Schematic image of EDA molecule in the interlayer space of CA/2-LDH (A), CA/3-LDH (B), CA/4-LDH (C) and CA/5-LDH (D).

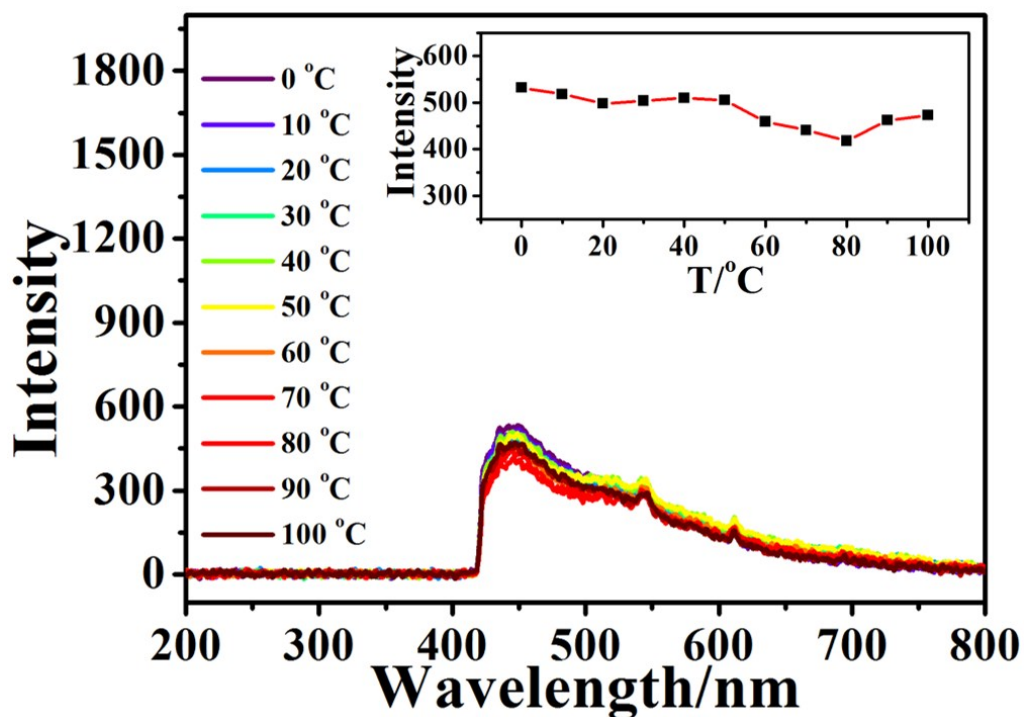


Figure S19. *In situ* fluorescence spectra of N-CDs/LDH in the temperature range from 0 to 100 °C; the inset shows the corresponding peak intensity as a function of temperature.

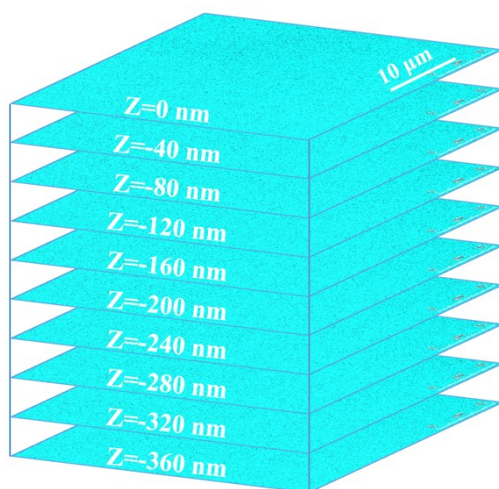


Figure S20. Confocal microscopy images of the N-CDs/LDH@PVA film with various film thickness.

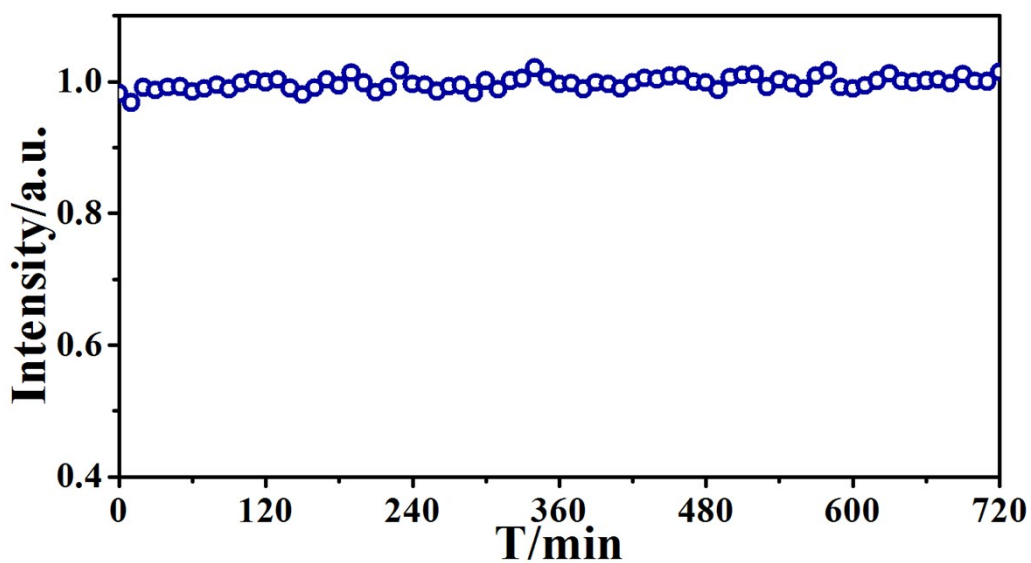


Figure S21. Stability of N-CDs/LDH@PVA film based BLED under operation conditions for 12 h.

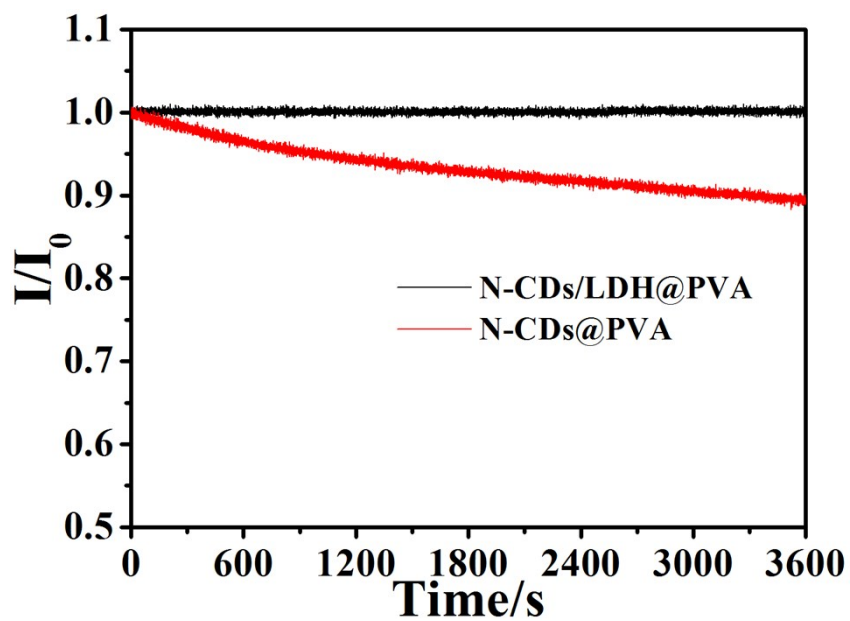


Figure S22. Photostability of the N-CDs@PVA film and N-CDs/LDH@PVA film upon irradiation by UV light (360 nm) for 3600 s.

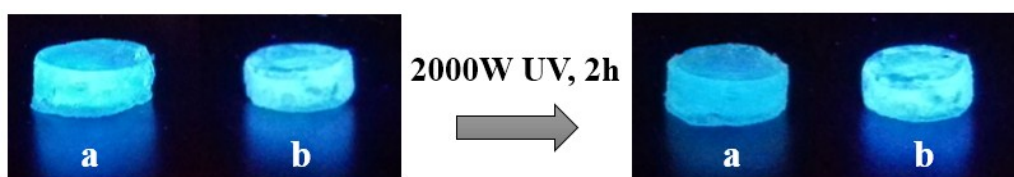


Figure S23. Photographs of N-CDs@PDMAA (a) and N-CDs/LDH@PDMAA (b) under high-power UV light for 2 h.

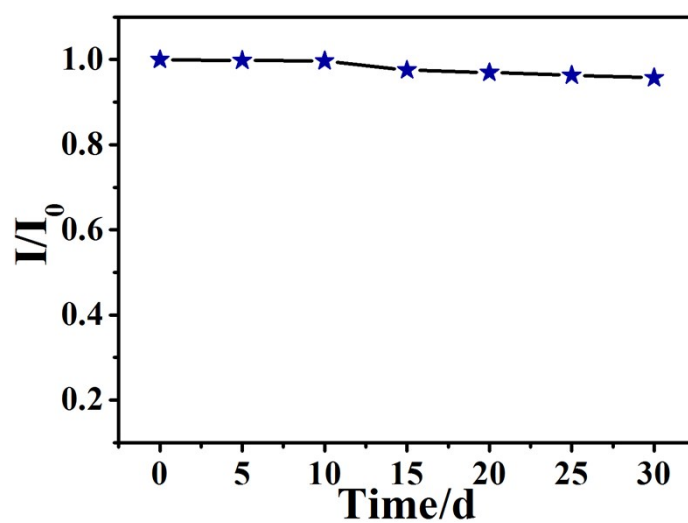


Figure S24. Fluorescence intensity of N-CDs/LDH recorded within 30 days.

Reference

- (1) Y. Zhao, F. Li, R. Zhang, D. G. Evans, X. Duan, *Chem. Mater.* 2002, **14**, 4286–4291.
- (2) A. S. Bookin, V. A. Drits, *Clays Clay Miner.* 1993, **41**, 551–557.
- (3) S. T. Zhang, H. Yan, M. Wei, D. G. Evans, X. Duan, *J. Phys. Chem. C* 2012, **116**, 3421–3431.
- (4) H. C. Andersen, *J. Chem. Phys.* 1980, **72**, 2384–2393.
- (5) H. J. C. Berendsen, J. P. M. Postma, W. F. Van Gunsteren, A. DiNola, J. R. Haak, *J. Chem. Phys.* 1984, **81**, 3684–3690.
- (6) M. P. Allen, D. J. Tildesley, *Computer Simulation of Liquids*; Clarendon: Oxford, U. K., 1987.
- (7) S. M. Xu, S. T. Zhang, W. Y. Shi, F. Y. Ning, Y. Fu, H. Yan, *RSC Adv.* 2014, **4**, 47472–47480.
- (8) D. Frenkel, B. Smit, *Understand Molecular Simulation: From Algorithms to Applications*, 2nd ed.; Academic Press: San Diego, 2002.
- (9) F. Wang, Z. Xie, H. Zhang, C. Y. Liu, Y. G. Zhang, *Adv. Funct. Mater.* 2011, **21**, 1027–1031.
- (10) D. Pan, J. Zhang, Z. Li, Z. Zhang, L. Guo, M. Wu, *J. Mater. Chem.* 2011, **21**, 3565–3567.
- (11) Z. Xie, F. Wang, C. Y. Liu, *Adv. Mater.* 2012, **24**, 1716–1721.
- (12) M. Xu, G. He, Z. Li, F. He, F. Gao, Y. Su, L. Zhang, Z. Yang, Y. Zhang, *Nanoscale* 2014, **6**, 10307–10315.
- (13) Y. Hao, Z. Gan, J. Xu, X. Wu, P. K. Chu, *Appl. Surf. Sci.* 2014, **311**, 490–497.
- (14) M. Sun, S. Qu, Z. Hao, W. Ji, P. Jing, H. Zhang, L. Zhang, J. Zhao, D. Shen, *Nanoscale* 2014, **6**, 13076–13081.

- (15) F. Wang, Z. Xie, B. Zhang, Y. Liu, W. Yang, C. Y. Liu, *Nanoscale* 2014, **6**, 3818–3823.
- (16) C. C. Shih, P. C. Chen, G. L. Lin, C. W. Wang, H. T. Chang, *ACS Nano* 2015, **9**, 312–319.
- (17) D. Mosconi, D. Mazzier, S. Silvestrini, A. Privitera, C. Marega, L. Franco, A. Moretto, *ACS Nano* 2015, **9**, 4156–4164.
- (18) C. Shen, J. Wang, Y. Cao, Y. Lu, *J. Mater. Chem. C* 2015, **3**, 6668–6675.
- (19) Y. Wang, S. Kalytchuk, L. Wang, O. Zhovtiuk, K. Cepe, R. Zboril, A. L. Rogach, *Chem. Commun.* 2015, **51**, 2950–2953.
- (20) Y. Chen, M. Zheng, Y. Xiao, H. Dong, H. Zhang, J. Zhuang, H. Hu, B. Lei, Y. Liu, *Adv. Mater.* 2016, **28**, 312–318.